

Extratropical shortwave cloud feedbacks in the context of the global circulation and hydrological cycle

Daniel T. McCoy¹, Paul Field², Michelle E. Frazer^{3,4}, Mark D. Zelinka⁵,
Gregory S. Elsaesser^{6,7}, Johannes Mülmenstädt⁸, Ivy Tan⁹, Timothy A.
Myers^{4,10}, Zachary J. Lebo¹

¹University of Wyoming

²United Kingdom Met Office

³Princeton University

⁴Pennsylvania State University

⁵Lawrence Livermore National Lab

⁶Columbia University

⁷Goddard Institute for Space Studies

⁸Pacific Northwest National Lab

⁹McGill University

¹⁰National Oceanic and Atmospheric Administration, Cooperative Institute for Research in
Environmental Sciences at the University of Colorado Boulder

Key Points:

- Enhanced moisture convergence with warming creates a negative extratropical cloud feedback.
- Cloud source and sink efficiency set the extratropical cloud response.
- Constraint by observations suggests a weakly negative feedback— and a moderate climate sensitivity.

Corresponding author: Daniel T. McCoy, daniel.mccoy@uwyo.edu

Abstract

Shortwave (SW) cloud feedback (SW_{FB}) is the primary driver of uncertainty in the effective climate sensitivity (ECS) predicted by global climate models (GCMs). ECS for several GCMs in the Sixth Coupled Model Intercomparison Project (CMIP6) exceed 5K, above the fifth assessment report (AR5) ‘likely’ maximum (4.5K) due to extratropical SW_{FB} ’s that are more positive than those simulated in previous generation CMIP5 GCMs. Here we show that across 57 GCMs Southern Ocean SW_{FB} can be predicted from the sensitivity of column-integrated liquid water mass (LWP) to moisture convergence and to surface temperature. The response of LWP to moisture convergence and the response of albedo to LWP anti-correlate across GCMs. This is because GCMs that simulate a larger response of LWP to moisture convergence tend to have higher mean-state LWPs, which reduces the impact of additional LWP on albedo. Observational constraints suggest a modestly negative Southern Ocean SW_{FB} — inconsistent with extreme ECS.

Plain Language Summary

As the climate warms, moisture convergence into the extratropics strengthens, increasing cloudiness, reflected sunlight, and precipitation. Increased cloudiness is set by how efficiently clouds form relative to precipitation depletion. Simulations where clouds form efficiently cannot reflect much more sunlight in the extratropics because they are already very cloudy and bright. Observations constrain both the sensitivity of reflected sunlight to cloud and of cloud to moisture. Combining these constraints with constraints on other cloud regimes rules out extremely small and large future warming.

1 Introduction

The SW cloud feedback (SW_{FB}) represents the central uncertainty in the future warming and effective climate sensitivity (ECS) predicted by GCMs. Uncertainty in SW_{FB} is a function of the parameterizations of cloud processes necessitated by the relatively coarse resolution of GCMs. Most GCMs transition from a positive SW_{FB} in the subtropics to a negative SW_{FB} poleward of 50°, albeit with substantial uncertainty in magnitude (Zelinka et al., 2016, 2020; Terai et al., 2016; Gordon & Klein, 2014). Several CMIP6 GCMs with very high ECS (>5K) have emerged owing to a more positive extratropical SW_{FB} (Frey & Kay, 2018; Zelinka et al., 2020; Bjordal et al., 2020) and this feature needs to be evaluated.

Different mechanisms have been put forward to explain negative extratropical SW_{FB} :

- Replacement of susceptible cloud ice with more reflective liquid (McCoy et al., 2014; Tsushima et al., 2006; Senior & Mitchell, 1993).
- Suppression of ice hydrometeor sinks of cloud through reduced glaciation (Tsushima et al., 2006; Ceppi, Hartmann, & Webb, 2016; McCoy et al., 2015; Field & Heymsfield, 2015; Mülmenstädt et al., 2021; Tan & Storelvmo, 2019; Kay et al., 2014).
- Enhanced air-sea exchange of aerosol precursors (Bodas-Salcedo et al., 2019).
- Strongly increasing adiabatic water content at cold temperatures (Betts & Harshvardhan, 1987; Terai et al., 2019).
- Increased extratropical moisture convergence driving enhanced condensation (McCoy et al., 2020, 2019).

We focus on the last of these processes. This is motivated by previous studies that found that changes in surface temperature (T_{skin}) and moisture convergence could be used to explain changes in extratropical cloudiness with minor contributions from other terms such as boundary layer stability and subsidence (McCoy et al., 2020).

It is difficult to untangle the effects of increased local T_{skin} on clouds as it may act through several of the processes listed above. One probable explanation is that increased T_{skin} acts to enhance buoyancy fluxes in the boundary layer, reducing cloud condensate (Bretherton & Blossey, 2014). This mechanism has been found to be important to boundary layer cloud changes across the subtropics (Klein et al., 2017; Myers & Norris, 2016; Myers et al., 2021). Here we treat T_{skin} variations as a proxy for all processes not related to moisture convergence.

SW_{FB} is essentially the change in upwelling SW (SW_{\uparrow}) due to clouds scaled by global mean temperature (GMT). We hypothesize that SW_{\uparrow} scales with albedo (α) and the proportionality

$$SW_{FB} \propto \frac{d\bar{\alpha}}{dGMT} \sim \frac{\partial\alpha}{\partial LWP} \cdot \frac{d\overline{LWP}}{dGMT} \quad (1)$$

holds. On the right hand side, the response of $\bar{\alpha}$ to GMT can be broken into the response of α to liquid water mass (LWP) and the response of \overline{LWP} to GMT. As discussed below, overbars denote regional means. We investigate and constrain GCM uncertainty in SW_{FB} terms on the right of Eq. 1.

2 Materials and Methods

Section 2.1 discussed the GCM data used in our analysis and Section 2.2 discusses the observational data used to constrain GCM behavior.

2.1 GCM analysis

The GCM variables examined are clivi (ice water path), clwvi (total cloud water path), pr (precipitation), hfes (evaporative flux), rsut (SW_{\uparrow}), rsutcs (clear-sky SW_{\uparrow}), ts (T_{skin}), and tas (2m air temperature). clwvi is the sum of ice water path (IWP) and LWP. We calculate LWP as clwvi-clivi.

For each GCM we analyze the pre-industrial control (piControl) and CO₂ quadrupling (abrupt4xCO2) simulations. The list of analyzed GCMs is given in the supplementary material (Table S1). The first 150 years of each simulation are examined, consistent with Sherwood et al. (2020).

The latitude range is 40-85°S unless otherwise stated. This is set by the region where zonal precipitation and evaporation difference ($P - E$) is consistently positive, which is similar across GCMs (Fig. S1). $P - E$ approximates moisture convergence when averaged over a large enough region (Held & Soden, 2006).

Our analysis is motivated in part by what variables can be well-observed in the extratropics. LWP is defined as the vertically-integrated mass of cloud liquid in a model grid cell, consistent with the microwave observations of cloud condensate (Elsaesser et al., 2017). Microwave LWP is insensitive to multi-layered clouds and does not have any dependence on sun-angle, making it optimal for observing clouds in the extratropics.

Cloud source processes are investigated in the HadGEM3 GCM by perturbing the cloud fraction scheme. HadGEM3 is as described in Mulcahy et al. (2018) and is run in atmosphere-only mode (the General Atmosphere 7.1, GA7.1). The only change from the base version of the model is to switch the cloud scheme from PC2 (Wilson et al., 2008) to Smith (Smith, 1990) because only one parameter needs to be perturbed in the latter.

110

2.2 Observations

111

112

113

114

115

116

117

118

119

120

MERRA-2 reanalysis (Molod et al., 2015) is used to characterize mean-state variability in $P-E$, T_{skin} , and 2m temperature. Observations of clear- and all-sky SW flux are taken from the CERES EBAF data set (Ed 4.1) for the period 2000-2016 (Wielicki et al., 1996). Observations of LWP are taken from MAC-LWP 1988-2016 (Elsaesser et al., 2017). MAC-LWP is a multi-satellite microwave column LWP record that is corrected for diurnal cycle artifacts and is directly comparable to GCM output without a satellite simulator (Bodas-Salcedo et al., 2011). However, microwave LWP is only available over open ocean (not over sea ice or land). The GCM output used in the main text are not filtered to remove land and sea ice to compare to existing SW_{FB} calculations (Zelinka et al., 2020). Resultant sampling uncertainty is evaluated below.

121

3 Results

122

123

124

125

126

127

128

129

130

131

132

133

134

135

136

137

138

At a regional scale the extratropics are characterized by convergence of moisture carried from the subtropics by transient eddies (e.g. extratropical cyclones) (Held & Soden, 2006; Hartmann, 2015; Yettella & Kay, 2017; Algarra et al., 2020; Guo et al., 2020). As shown in Held and Soden (2006), global warming drives enhanced moisture convergence in this region. Moisture convergence is represented, as in previous work, as $P-E$. As in McCoy et al. (2020), we consider a steady-state model of the extratropical atmosphere. In this framework increased moisture convergence is balanced by increased precipitation. The conversion of vapor to precipitation happens in clouds and increased moisture convergence drives increased cloudiness. This is shown schematically in Fig. 1. In this framework the diversity of model responses is driven by the complexity of parameterizing subgrid-scale condensation and precipitation processes. Rates of creation and removal of cloud are considered in terms of efficiency of cloud sources (e_{source}) and sinks (e_{sink}) and the reservoirs of vapor and condensed water (Fig. 1a). The response of the extratropics to global warming is characterized by increased moisture convergence (Fig. 1b). In models where sources are efficient relative to sinks this leads to sharp increases in cloud and a relatively strong negative cloud feedback. If the efficiencies are reversed the negative cloud feedback is weak (Fig. 1c) (McCoy et al., 2020).

139

3.1 Changes in liquid cloud

140

141

142

143

144

In this section we characterize the dependence of extratropical liquid water path (LWP) on moisture convergence ($P-E$) and surface temperature (T_{skin}) to predict $dLWP/dGMT$ (Eq. 1). (Note average of quantities over 40°-85°S are denoted $\overline{(\)}$.) GCMs predictions of LWP vary by an order of magnitude (Fig. S2), while $P-E$ varies by only a factor of three (Fig. S1).

145

146

147

As discussed in Section 2.2, LWP is column-integrated all-sky liquid mass, in contrast to focusing on low-topped clouds (Myers et al., 2021). This allows comparison between GCM output and microwave radiometer observations (Elsaesser et al., 2017).

148

149

150

151

152

153

154

155

We choose $\overline{P-E}$ and $\overline{T_{skin}}$ as cloud controlling factors (Stevens & Brenguier, 2009) based on previous analysis that found that within a given meteorological regime horizontal moisture convergence and sea surface temperature dominated the predicted change in extratropical LWP across a suite of GCMs (McCoy et al., 2020, 2019). The effect of neglecting other predictors in this study will be evaluated by prediction of out-of-sample future simulations, as in Qu et al. (2015). The approximation of moisture convergence as $P-E$ ignores advection out of the atmospheric column and zonal averaging is used to account for zonal advection over the Southern Ocean (Seager & Henderson, 2013).

156

In each GCM, the multiple linear regression model

$$\overline{LWP} = b_1 \cdot \overline{P - E} + b_2 \cdot \overline{T_{skin}} + b_3 \quad (2)$$

157 is trained in the piControl simulation and used to predict the abrupt4xCO2 simulation.
 158 This follows the approach used to constrain subtropical cloud feedback in Qu et al. (2015).
 159 As discussed in Qu et al. (2015), predictor correlation between cloud controlling factors
 160 can be problematic when $R^2 > 0.9$ between predictors. The strongest correlation be-
 161 tween predictors in our study was $R^2 = 0.6$.

162 One of the assumptions inherent to cloud controlling factor predictions is that the
 163 relationship between clouds and meteorological factors is unchanged between the climate
 164 mean-state and future warmed climates, referred to as 'time-scale invariance' (Klein et
 165 al., 2017). We evaluate whether the predictors in Eq. 2 are time-scale invariant in the
 166 context of the GCMs. As in Qu et al. (2015), we contrast coefficients derived in mean-
 167 state and warmed simulations. The predictors in Eq. 2 are consistent when inferred from
 168 piControl or from abrupt4xCO2 simulations (Fig. S3).

169 Eq. 2 predicts extratropical LWP. Extratropical moisture convergence is driven by
 170 local flux and tropical export (Hartmann, 2015; Algarra et al., 2020). SW_{FB} is typically
 171 given as the feedback on global, rather than regional, mean temperature. Thus we write
 172 the prediction of LWP response to GMT as:

$$\frac{d\overline{LWP}}{dGMT} = b_1 \cdot \frac{d\overline{P - E}}{dGMT} + b_2 \cdot \frac{d\overline{T_{skin}}}{dGMT} + b_3 \quad (3)$$

173 $\overline{dP - E}/dGMT$, and $\overline{dT_{skin}}/dGMT$ are quantified as the linear regression of annual-
 174 mean $\overline{P - E}$, and $\overline{T_{skin}}$ on GMT for the first 150 years of abrupt4xCO2. b_{1-3} are cal-
 175 culated using multiple linear regression on monthly-mean piControl output using Eq. 2.

176 The changes in LWP predicted by Eq. 3 agree with the abrupt4xCO2 simulations
 177 (Fig. 2). The correlation between abrupt4xCO2 $d\overline{LWP}/dGMT$ and the prediction based
 178 on Eq. 3 is $r = 0.71$, and predictions fall along the 1-1 line (see discussion below). Fit
 179 lines in Fig. 2 are calculated using orthogonal regression with uncertainty in both pre-
 180 dictors and predictands. The 95% confidence range on the intercept and slope of the best
 181 fit line are calculated using Jackknife resampling (Tukey, 1958). Uncertainty is propa-
 182 gated from uncertainty in b_{1-3} and uncertainty in $d\overline{P - E}/dGMT$ and $d\overline{T_{skin}}/dGMT$.

183 Several GCMs that share the same cloud physics (CESM2, CESM2-FV, CESM2-
 184 WACCM, WACCM-FV, E3SM-1-0) are excluded from the fit in Fig. 2. These GCMs
 185 are unique in only increasing extratropical LWP in the first 15 years of the abrupt4xCO2
 186 simulation followed by decreasing LWP (Bjordal et al., 2020) (Fig. S4). The extratrop-
 187 ical cloud response of CESM2 is an active area of investigation at this time and may re-
 188 lated to the treatment of ice in the cloud physics parameterization (Bjordal et al., 2020).

189 An observational constraint on $d\overline{LWP}/dGMT$ is calculated by training Eq. 2 on
 190 observations from microwave radiometers (Elsaesser et al., 2017) and reanalysis from MERRA-
 191 2 (Molod et al., 2015). Observed b_{1-3} (Eq. 2, see Fig. S3) is combined with $d\overline{P - E}/dGMT$
 192 and $d\overline{T_{skin}}/dGMT$ for each GCM following Eq. 3. Uncertainty is propagated from un-
 193 certainty in b_{1-3} , but is dominated by spread between GCMs in $d\overline{P - E}/dGMT$ and $d\overline{T_{skin}}/dGMT$.

194 Microwave LWP is only available over open water (Wentz & Meissner, 2000). We
 195 quantify the sampling error due to neglecting data over ice and land. Predicted $d\overline{LWP}/dGMT$
 196 for GCMs when the regression model (Eq. 2) is trained using only data over open wa-
 197 ter is contrasted with the value when all data is used. Monthly values on the native grid
 198 of the GCM where $\alpha_{clear-sky} > 0.4$ are excluded to remove ice and land. The zonal-,
 199 latitudinal-, monthly-means calculated from the filtered data are used to train Eq. 2. The
 200 constraint on $d\overline{LWP}/dGMT$ is not strongly affected by only considering open ocean (Fig.
 201 S5) and sampling error is included in the constraint in Fig. 2.

The median value and standard deviation of $\overline{dP - E}/dGMT$ across GCMs is $0.77 \pm 0.39 \text{ W m}^{-2} \text{ K}^{-1}$. For $\overline{dT_{Skin}}/dGMT$ it is $1.19 \pm 0.36 \text{ K/K}$. The relative contribution to $\overline{dLWP}/dGMT$ by changes in $\overline{P - E}$ has a median value of 15% across GCMs but ranges from 0% up to 250% (values greater than 100% occur in GCMs where contributions from surface warming and moistening have opposing effects on \overline{LWP}).

Combining the observational constraint on $\overline{dLWP}/dGMT$ with the best fit line in Fig. 2 yields a constraint on $\overline{dLWP}/dGMT$ ranging from $0.9 \cdot 10^{-3}$ to $3 \cdot 10^{-3} \text{ kg} \cdot \text{m}^{-2} \text{ K}^{-1}$. Direct comparison to other studies is difficult given differing study regions, lack of regime-partitioning, temporal-averaging and configurations of the warming signal, but qualitatively there is agreement regarding an increase in extratropical LWP in response to warming, albeit weaker than most GCMs (Fig. S2) (Ceppi, McCoy, & Hartmann, 2016; Manaster et al., 2017; McCoy et al., 2020, 2019; Ceppi & Nowack, 2021).

Based on our analysis, we find that extratropical LWP changes in response to warming across many GCMs can be predicted based on their present-day, monthly covariability between Southern Ocean LWP, moisture convergence, and T_{Skin} . Given that these terms are among the simplest descriptors of atmospheric state (is the atmosphere warm on the bottom and is it moist), this is not too unexpected.

3.2 Compensation between moisture removal and radiative efficiency across GCMs

We now consider the radiative sensitivity term $\partial\alpha/\partial LWP$ from Eq. 1. Because LWP integrates over cloudy and clear regions (Elsaesser et al., 2017) it is an emergent property of a complex population of clouds. To first order, the relation between LWP and SW_{\uparrow} is a function of cloud areal extent (Bender et al., 2017), cloud optical thickness (Gordon & Klein, 2014), and the underlying surface properties (increased cloud will affect SW_{\uparrow} more over a dark surface). To quantify how SW_{\uparrow} responds to changes in LWP, we train the following multiple linear regression model relating albedo (α) to LWP and clear-sky α ($\alpha_{clear-sky}$)

$$\alpha = c_1 \cdot LWP + c_2 \cdot \alpha_{clear-sky} + c_3 \quad (4)$$

where $\alpha = SW_{\uparrow}/SW_{\downarrow}$ is calculated from monthly means of top-of-atmosphere flux. (Note the lack of overbars in Eq. 4. This is because a regional average is not required as it is in Eq. 2 to make $P - E$ a reasonable approximation for moisture convergence.) The regression model in Eq. 4 is trained on data 40-85°S at the native resolution of each GCM. It is trained independently in each calendar month due to residual effects from the seasonal cycle of solar zenith angle, which strongly affects α (McCoy et al., 2018). The regression model in Eq. 4 could easily be improved, for instance by including information about ice water path, but we have chosen to consider variables that can be quantified accurately in observations and that are available from GCMs (Jiang et al., 2012)—in this case LWP and SW_{\uparrow} .

The sensitivity of α to LWP ($\partial\alpha/\partial LWP$) derived from piControl simulations is inversely related to the mean-state LWP (Fig. 3). Albedo and cloud fraction (the areal coverage of cloud, CF) are nearly linearly related (Bender et al., 2017), but the effects of in-cloud LWP ($LWP_{in-cloud}$) on α saturates at high $LWP_{in-cloud}$ (Liou, 2002; Lacis & Hansen, 1974). LWP includes information about $LWP_{in-cloud}$ and cloud extent ($LWP \approx CF \cdot LWP_{in-cloud}$); thus, as the LWP across the extratropics increases, liquid begins to affect SW_{\uparrow} less efficiently by increasing liquid water density in cloud rather than filling in cloud cover. This leads to the saturation in $\partial\alpha/\partial LWP$ as a function of increasing mean-state LWP.

Eq. 4 is trained on observations from CERES and MAC-LWP to yield an observational estimate of $\partial\alpha/\partial LWP$. The $\partial\alpha/\partial LWP$ estimated from observations falls along

the relation between mean-state LWP and $\partial\alpha/\partial LWP$ emerging from GCMs (Fig. 3). This is encouraging as it suggests that the relationship between LWP and α is based on radiative transfer and distributions of cloud that are well-represented in GCMs (time-scale invariance is shown in Fig. S3). $\partial\alpha/\partial LWP$ inferred from observations is on the lower end of the $\partial\alpha/\partial LWP$ in GCMs. The finding that GCM SW_{\uparrow} is too sensitive to LWP is consistent with previous studies (Kelleher & Grise, 2019).

The sensitivity of LWP to converging moisture ($\overline{\partial LWP/\partial P - E}$, Eq. 2) correlates positively with mean-state LWP (Fig. 3). The sensitivity of LWP to T_{skin} ($\overline{\partial LWP/\partial T_{skin}}$) does not correlate with mean-state LWP, and 95% of GCMs fall between $-0.0001 kg \cdot m^{-2} K^{-1}$ and $0.007 kg \cdot m^{-2} K^{-1}$. Observations infer $\overline{\partial LWP/\partial T_{skin}} = 0.0006 \pm 0.0001 kg \cdot m^{-2} K^{-1}$. The diagnosed relationship relating LWP to T_{skin} is likely to represent several processes (Terai et al., 2019). We focus on $\overline{\partial LWP/\partial P - E}$ because of its emergent relationship with mean-state LWP.

The relationship between $\overline{\partial LWP/\partial P - E}$ and mean-state \overline{LWP} shown in Fig. 3 can be explained in the framework of sources and sinks of cloud (Fig. 1). LWP will be high when sources of cloud are efficient relative to sinks. Further, LWP will be sensitive to increased moisture convergence (a large $\overline{\partial LWP/\partial P - E}$). However, radiation will be insensitive to increased LWP (a small $\partial\alpha/\partial LWP$) because the extratropics will already be extremely cloudy ($CF \approx 1$) and thus there will be relatively few clear patches that can be filled in for maximum radiative effect. Instead, overcast regions must increase in-cloud liquid content for diminishing returns in SW_{\uparrow} .

We test the hypothesis that the dependence of $\overline{\partial LWP/\partial P - E}$ and $\partial\alpha/\partial LWP$ on mean-state \overline{LWP} is a function of varying cloud source and sink strength using HadGEM3 run in atmosphere-only mode (Mulcahy et al., 2018) with the Smith cloud scheme (Smith, 1990), which uses a critical relative humidity (RH_{crit}) (Quaas, 2012; Smith, 1990). Use of the Smith cloud scheme allows us to represent the strength of the source term using a single parameter (RH_{crit}). RH_{crit} is varied from 100% (clouds are only formed when the GCM grid box has total relative humidity $>100\%$) to 20%. The mean-state pattern of $P - E$ changes dramatically for $RH_{crit} < 80\%$. To provide a fair comparison to the coupled GCMs we examine the latitude range in each HadGEM3 simulation where climatological, zonal-mean $P - E$ is positive as opposed to selecting 40-85°S, as in the coupled GCMs (see Fig. S1). The dependence of $\overline{\partial LWP/\partial P - E}$ and $\partial\alpha/\partial LWP$ on mean-state LWP derived from the HadGEM3 simulations agrees with the behavior of the coupled GCMs. As RH_{crit} decreases (stronger cloud source) $\overline{\partial LWP/\partial P - E}$ increases and $\partial\alpha/\partial LWP$ decreases. This supports our hypothesis that the relative efficiency of sources and sinks in GCMs affect mean-state cloud, the response of extratropical cloud to increased moisture convergence, and the effect of increased cloud on SW_{\uparrow} .

In summary, strong responses of LWP to moisture convergence in warming simulations are compensated by weak increases in SW_{\uparrow} in response to LWP. The relationships in Fig. 3 may provide a useful process-level constraint on GCMs.

3.3 Constraints on SW cloud feedback

In the preceding sections we provided constraints on the terms on the right-hand-side of Eq. 1. We now combine these constraints to provide a constraint on SW_{FB} following Eq. 1. It is found that Eq. 1 using values from Fig. 2 and 3 predicts SW_{FB} across GCMs (Fig. 4a). The term $\partial\alpha/\partial LWP$ is calculated using December values (when insolation is strong, Eq. 4).

The prediction of SW_{FB} for three regions by 40-85°S $\overline{dLWP/dGMT}$ and $\partial\alpha/\partial LWP$ is shown. Moistening is not uniform across the 40-85°S region (Fig. S1). LWP is reduced in the 40-50°S region consistent with Hadley cell expansion and drying (Kay et al., 2014; Tselioudis et al., 2016; Grise & Medeiros, 2016; Lu et al., 2007; Sousa et al., 2018; Kelle-

her & Grise, 2021) (Fig. S1) and SW_{FB} tends to be positive in this region (Fig. 4a). In the 50-85°S region there is consistent moistening (Fig. S1), LWP increases (Fig. S2), and SW_{FB} tends to be negative (Fig. 4a). The prediction of SW_{FB} averaged 40-85°S is the area-weighted sum of these effects. Clearly, influence on the region of moistening by Hadley cell expansion modulates extratropical SW_{FB} (Kelleher & Grise, 2021).

Prediction of Hadley cell expansion is beyond the scope of this work. Thus, we examine the region of consistent moistening. Eq. 1 explains 83% of the variance in SW_{FB} averaged between 50-85°S (Fig. 4a). The observational constraints on the right hand side of Eq. 1 predicts the contribution to global-mean SW_{FB} from the 50°S-85°S region to be between $-0.1 Wm^{-2}K^{-1}$ to $0.0 Wm^{-2}K^{-1}$, consistent with the interpretation of Eq. 1 as an emergent constraint on 50°S-85°S SW_{FB} (Klein & Hall, 2015; Hall & Qu, 2006). In summary, SW_{FB} is negative in regions of moistening.

3.4 Conclusion and probable range of ECS

How does the constraint on SW_{FB} from Eq. 1 inform the most probable range for ECS? For illustrative purposes we detail a simple constraint. The ECS calculated from 71 CMIP5 and CMIP6 models (Zelinka et al., 2020)¹ is constrained by 50-85°S (extratropical moistening regime) and 35°S-35°N (subtropical) cloud feedback (Fig. 4b). The subtropical marine, low-topped cloud feedback is examined for consistency with previous studies (Myers et al., 2021). The number of GCMs is increased here because some GCMs did not have all the necessary variables to examine moisture and cloud changes. The subtropical and extratropical SW_{FB} are considered simultaneously because subtropical cloud feedback is a key uncertainty (Bony, 2005; Myers & Norris, 2016; Bretherton & Caldwell, 2020).

More positive cloud feedback in either averaging region corresponds to higher ECS. Subtropical and extratropical cloud feedbacks are correlated across GCMs (Fig. 4b). This has been noted before (McCoy et al., 2016), but the physical reason for this behavior in GCMs is not clear.

Constraining GCMs to be consistent with constraints on either regional cloud feedback doesn't substantially narrow ECS (Fig. 4c). Consideration of both constraints results in ECS falling between 2.6K and 4.8K with a median of 4.3K. No GCMs with ECS $< 2.5K$ or $> 5K$ out of the original 71 GCMs are consistent with constraints on both subtropical and extratropical cloud feedback and the means differ at 95% confidence using a Welch's t-test. However, this approach is sensitive to the prior distribution from GCMs.

We calculate a more rigorous constraint on ECS using the World Climate Research Programme (WCRP) Bayesian framework (Sherwood et al., 2020). In Sherwood et al. (2020) process-level understanding of cloud feedbacks from the literature was evaluated and the most likely ranges for cloud feedback in various geographic regions and cloud regimes were input into a Bayesian model along with other constraints on ECS, such as paleoclimate records. The cloud feedbacks in the 50°-85° regions considered by Sherwood et al. (2020) were: 40°-70° cloud optical depth set at $0.0 Wm^{-2}K^{-1}$ with $\sigma \pm 0.1$ and middle latitude (30°-60°) marine low cloud set at $+0.08 \pm 0.08 Wm^{-2}K^{-1}$. All other potential cloud feedbacks in the 50°-85° region were assumed to be $0.0 \pm 0.0 Wm^{-2}K^{-1}$ because of insufficient process-level understanding and constraints.

Summing the different probable feedback values from Sherwood et al. (2020) for the 50°S-85°S region (assuming all feedbacks are constant in their given latitude ranges) gives a value of $+0.01 \pm 0.03 Wm^{-2}K^{-1}$, or at 95% $\pm 0.06 Wm^{-2}K^{-1}$. Both Sherwood

¹ https://github.com/mzelinka/cmip56_forcing_feedback_ecs

347 et al. (2020) and Fig. 4 suggest very negative extratropical cloud feedbacks are unlikely.
 348 However, Fig. 4 infers the most likely value of SW_{FB} to be negative because it does not
 349 neglect non-boundary layer cloud, or cloud poleward of 70° , for which GCMs consistently
 350 predict a negative SW_{FB} (Zelinka et al., 2016; Terai et al., 2016; Ceppi, McCoy, & Hart-
 351 mann, 2016).

352 The latitude range used in the WCRP assessment algorithm for the extratropical
 353 region (oceans 60° - 90° in both hemispheres) differs slightly from our analysis of the uni-
 354 form moistening in the Southern Ocean (50 - 85° S). To use the existing WCRP code we
 355 need to offer a prediction for the 60 - 90° oceans. Using the predictor in Fig. 4 for 60 - 90° yields
 356 a similar prediction (Fig. S6) to those shown in Fig. 4a. Combining this value with the
 357 constraint provided by Myers et al. (2021) results in a global constraint on marine cloud
 358 feedback. This is used to update the likelihood of ECS from Sherwood et al. (2020) of
 359 3.11K (95% confidence: 2.26 - 4.70K) to 2.86K (95% confidence: 2.13 - 4.12K). The prob-
 360 ability of ECS above the 4.5K upper end of the AR5 likely range becomes increasingly
 361 unlikely falling from 6.6% (Sherwood et al., 2020), to 2.3% when using constraints on
 362 global marine cloud feedback.

363 Our analysis points to enhanced moisture convergence in the extratropics as a key
 364 driver of enhanced cloud condensate and negative feedback in this region. The control
 365 on where moistening occurs exerted by Hadley cell expansion is found to be an impor-
 366 tant modulator of extratropical SW_{FB} . The response of cloud to moisture convergence
 367 is presented in a source-sink framework (Fig. 1). Because strong sources push the ex-
 368 tratropics to be very cloudy, this results in compensation between the effects of increased
 369 moisture on cloud and increased cloud on radiation (Fig. 3). The terms in Fig 3 can pro-
 370 vide a useful process constraint for GCMs and observations of both radiative efficiency
 371 and cloud response to meteorology suggest that extratropical SW_{FB} in regions of moist-
 372 ening is negative, albeit not as negative as predicted by many GCMs (Fig. 4a). Over-
 373 all, extreme ECS is not consistent with observationally-constrained extratropical SW_{FB}
 374 when combined with other lines of evidence (Sherwood et al., 2020; Myers et al., 2021)
 375 (Fig. 4bc).

376 Acknowledgments

377 **Funding** DTM and PRF acknowledge support from the Process-Based Climate Sim-
 378 ulation: Advances in High- Resolution Modelling and European Climate Risk Assess-
 379 ment (PRIMAVERA) project funded by the European Union’s Horizon 2020 program
 380 under Grant Agreement 641727. DTM acknowledges support from the University of Wyoming.
 381 IT acknowledges support from NSERC RGPIN-2021-02720. The work of MDZ was per-
 382 formed under the auspices of the U.S. Department of Energy (DOE) by Lawrence Liv-
 383 ermore National Laboratory under Contract DE-AC52-07 NA27344 and was supported
 384 by the Regional and Global Model Analysis Program of the Office of Science at the DOE.
 385 JM was supported by the Atmospheric System Research (ASR) program as part of the
 386 DOE Office of Biological and Environmental Research. Pacific Northwest National Lab-
 387 oratory is operated by Battelle Memorial Institute for the U.S. Department of Energy.
 388 MEF was supported by National Science Foundation award AWD1005319. **Data avail-**
 389 **ability** All CMIP data are archived at esgf-node.llnl.gov/projects/esgf-llnl/. Output from
 390 GA7.1 using the Smith scheme are accessed through the data server at the JASMIN Cen-
 391 tre for European Data Analysis using the Moose archive interface ([https://gws-access](https://gws-access.jasmin.ac.uk/public/mohc_shared/moose-user-doc/external_user_guide.html)
 392 [.jasmin.ac.uk/public/mohc_shared/moose-user-doc/external_user_guide.html](https://gws-access.jasmin.ac.uk/public/mohc_shared/moose-user-doc/external_user_guide.html)).
 393 The permanent access numbers are: 'u-bt821', 'u-bt845', 'u-bt848', 'u-bt850', 'u-bt819',
 394 'u-bt852'. MAC-LWP data can be accessed at [https://disc.gsfc.nasa.gov/datasets/](https://disc.gsfc.nasa.gov/datasets/MACLWP_diurnal_1/summary?keywords=measures)
 395 [MACLWP_diurnal_1/summary?keywords=measures](https://disc.gsfc.nasa.gov/datasets/MACLWP_diurnal_1/summary?keywords=measures). MERRA-2 data are available at [https://](https://disc.gsfc.nasa.gov/datasets/M2TMNXSLV_5.12.4/summary?keywords=MERRA2)
 396 disc.gsfc.nasa.gov/datasets/M2TMNXSLV_5.12.4/summary?keywords=MERRA2.

References

- 397
- 398 Algarra, I., Nieto, R., Ramos, A. M., Eiras-Barca, J., Trigo, R. M., & Gimeno, L.
 399 (2020, October). Significant increase of global anomalous moisture uptake
 400 feeding landfalling Atmospheric Rivers. *Nature Communications*, *11*(1), 5082.
 401 doi: 10.1038/s41467-020-18876-w
- 402 Bender, F. A. M., Engström, A., Wood, R., & Charlson, R. J. (2017, June). Evaluation
 403 of Hemispheric Asymmetries in Marine Cloud Radiative Properties. *Journal of Climate*,
 404 *30*(11), 4131–4147. doi: 10.1175/JCLI-D-16-0263.1
- 405 Betts, A. K., & Harshvardhan. (1987, July). THERMODYNAMIC CONSTRAINT
 406 ON THE CLOUD LIQUID WATER FEEDBACK IN CLIMATE MOD-
 407 ELS. *Journal of Geophysical Research-Atmospheres*, *92*(D7), 8483–8485.
 408 doi: 10.1029/JD092iD07p08483
- 409 Bjordal, J., Storelvmo, T., Alterskjær, K., & Carlsen, T. (2020, November).
 410 Equilibrium climate sensitivity above 5 °C plausible due to state-
 411 dependent cloud feedback. *Nature Geoscience*, *13*(11), 718–721. doi:
 412 10.1038/s41561-020-00649-1
- 413 Bodas-Salcedo, A., Mulcahy, J. P., Andrews, T., Williams, K. D., Ringer, M. A.,
 414 Field, P. R., & Elsaesser, G. S. (2019). Strong Dependence of Atmospheric
 415 Feedbacks on Mixed-Phase Microphysics and Aerosol-Cloud Interactions in
 416 HadGEM3. *Journal of Advances in Modeling Earth Systems*, *0*(0). doi:
 417 10.1029/2019ms001688
- 418 Bodas-Salcedo, A., Webb, M. J., Bony, S., Chepfer, H., Dufresne, J. L., Klein, S. A.,
 419 ... John, V. O. (2011, August). COSP: Satellite simulation software for model
 420 assessment. *Bulletin of the American Meteorological Society*, *92*(8), 1023–1043.
 421 doi: 10.1175/2011BAMS2856.1
- 422 Bony, S. (2005). Marine boundary layer clouds at the heart of tropical cloud feed-
 423 back uncertainties in climate models. *Geophysical Research Letters*, *32*(20).
 424 doi: 10.1029/2005gl023851
- 425 Bretherton, C. S., & Blossey, P. N. (2014). Low cloud reduction in a greenhouse-
 426 warmed climate: Results from Lagrangian LES of a subtropical marine cloudi-
 427 ness transition. *Journal of Advances in Modeling Earth Systems*, *6*(1), 91–114.
 428 doi: 10.1002/2013MS000250
- 429 Bretherton, C. S., & Caldwell, P. M. (2020, September). Combining Emergent Con-
 430 straints for Climate Sensitivity. *Journal of Climate*, *33*(17), 7413–7430. doi: 10
 431 .1175/JCLI-D-19-0911.1
- 432 Ceppi, P., Hartmann, D. L., & Webb, M. J. (2016). Mechanisms of the Negative
 433 Shortwave Cloud Feedback in Middle to High Latitudes. *Journal of Climate*,
 434 *29*(1), 139–157. doi: doi:10.1175/JCLI-D-15-0327.1
- 435 Ceppi, P., McCoy, D. T., & Hartmann, D. L. (2016). Observational evidence for a
 436 negative shortwave cloud feedback in middle to high latitudes. *Geophysical Re-
 437 search Letters*, *43*(3), 1331–1339. doi: 10.1002/2015gl067499
- 438 Ceppi, P., & Nowack, P. (2021, July). Observational evidence that cloud feedback
 439 amplifies global warming. *Proceedings of the National Academy of Sciences*,
 440 *118*(30), e2026290118. Retrieved from [http://www.pnas.org/content/118/
 441 30/e2026290118.abstract](http://www.pnas.org/content/118/30/e2026290118.abstract) doi: 10.1073/pnas.2026290118
- 442 Elsaesser, G. S., O'Dell, C. W., Lebsock, M. D., Bennartz, R., Greenwald, T. J.,
 443 & Wentz, F. J. (2017). The Multi-Sensor Advanced Climatology of
 444 Liquid Water Path (MAC-LWP). *Journal of Climate*, *0*(0), null. doi:
 445 10.1175/jcli-d-16-0902.1
- 446 Field, P. R., & Heymsfield, A. J. (2015). Importance of snow to global precip-
 447 itation. *Geophysical Research Letters*, *42*(21), 9512–9520. doi: 10.1002/
 448 2015GL065497
- 449 Frey, W. R., & Kay, J. E. (2018, April). The influence of extratropical cloud phase
 450 and amount feedbacks on climate sensitivity. *Climate Dynamics*, *50*(7), 3097–
 451 3116. doi: 10.1007/s00382-017-3796-5

- 452 Gordon, N. D., & Klein, S. A. (2014). Low-cloud optical depth feedback in climate
453 models. *Journal of Geophysical Research: Atmospheres*, *119*(10), 6052–6065.
454 doi: 10.1002/2013JD021052
- 455 Grise, K. M., & Medeiros, B. (2016, December). Understanding the Varied Influence
456 of Midlatitude Jet Position on Clouds and Cloud Radiative Effects in Observa-
457 tions and Global Climate Models. *Journal of Climate*, *29*(24), 9005–9025. doi:
458 10.1175/JCLI-D-16-0295.1
- 459 Guo, Y., Shinoda, T., Guan, B., Waliser, D. E., & Chang, E. K. M. (2020). Sta-
460 tistical Relationship between Atmospheric Rivers and Extratropical Cy-
461 clones and Anticyclones. *Journal of Climate*, *33*(18), 7817–7834. doi:
462 10.1175/JCLI-D-19-0126.1
- 463 Hall, A., & Qu, X. (2006, February). Using the current seasonal cycle to constrain
464 snow albedo feedback in future climate change. *Geophysical Research Letters*,
465 *33*(3). Retrieved 2021-09-04, from <https://doi.org/10.1029/2005GL025127>
466 (Publisher: John Wiley & Sons, Ltd) doi: 10.1029/2005GL025127
- 467 Hartmann, D. L. (2015). *Global physical climatology* (Vol. 103). Newnes.
- 468 Held, I. M., & Soden, B. J. (2006, November). Robust responses of the hydrological
469 cycle to global warming. *Journal of Climate*, *19*(21), 5686–5699. doi: 10.1175/
470 jcli3990.1
- 471 Jiang, J. H., Su, H., Zhai, C., Perun, V. S., Del Genio, A., Nazarenko, L. S., ...
472 Stephens, G. L. (2012). Evaluation of cloud and water vapor simulations
473 in CMIP5 climate models using NASA “A-Train” satellite observations.
474 *Journal of Geophysical Research: Atmospheres*, *117*(D14), D14105. doi:
475 10.1029/2011JD017237
- 476 Kay, J. E., Medeiros, B., Hwang, Y. T., Gettelman, A., Perket, J., & Flanner,
477 M. G. (2014). Processes controlling Southern Ocean shortwave climate
478 feedbacks in CESM. *Geophysical Research Letters*, 2013GL058315. doi:
479 10.1002/2013GL058315
- 480 Kelleher, M. K., & Grise, K. M. (2019). Examining Southern Ocean Cloud
481 Controlling Factors on Daily Time Scales and Their Connections to Mid-
482 latitude Weather Systems. *Journal of Climate*, *32*(16), 5145–5160. doi:
483 10.1175/jcli-d-18-0840.1
- 484 Kelleher, M. K., & Grise, K. M. (2021, October). Varied midlatitude shortwave
485 cloud radiative responses to Southern Hemisphere circulation shifts. *At-
486 mospheric Science Letters*, *n/a*(*n/a*), e1068. Retrieved 2021-11-24, from
487 <https://doi.org/10.1002/asl.1068> (Publisher: John Wiley & Sons, Ltd)
488 doi: 10.1002/asl.1068
- 489 Klein, S. A., & Hall, A. (2015). Emergent Constraints for Cloud Feedbacks. *Current
490 Climate Change Reports*, *1*(4), 276–287. doi: 10.1007/s40641-015-0027-1
- 491 Klein, S. A., Hall, A., Norris, J. R., & Pincus, R. (2017, November). Low-Cloud
492 Feedbacks from Cloud-Controlling Factors: A Review. *Surveys in Geophysics*,
493 *38*(6), 1307–1329. doi: 10.1007/s10712-017-9433-3
- 494 Lacis, A. A., & Hansen, J. E. (1974). PARAMETERIZATION FOR ABSORP-
495 TION OF SOLAR-RADIATION IN EARTH'S ATMOSPHERE. *Journal of the
496 Atmospheric Sciences*, *31*(1), 118–133. doi: 10.1175/1520-0469(1974)031<0118:
497 apftao>2.0.co;2
- 498 Liou, K.-N. (2002). *An introduction to atmospheric radiation*. Elsevier.
- 499 Lu, J., Vecchi, G. A., & Reichler, T. (2007, March). Expansion of the Hadley cell
500 under global warming. *Geophysical Research Letters*, *34*(6). Retrieved 2021-
501 11-06, from <https://doi.org/10.1029/2006GL028443> (Publisher: John Wil-
502 ley & Sons, Ltd) doi: 10.1029/2006GL028443
- 503 Manaster, A., O'Dell, C. W., & Elsaesser, G. (2017). Evaluation of Cloud Liquid
504 Water Path Trends Using a Multidecadal Record of Passive Microwave Obser-
505 vations. *Journal of Climate*, *30*(15), 5871–5884. doi: 10.1175/jcli-d-16-0399.1
- 506 McCoy, D. T., Field, P., Bodas-Salcedo, A., Elsaesser, G. S., & Zelinka, M. D.

- (2020). A regime-oriented approach to observationally constraining extratropical shortwave cloud feedbacks. *Journal of Climate*, 1–55. doi: 10.1175/JCLI-D-19-0987.1
- McCoy, D. T., Field, P. R., Elsaesser, G. S., Bodas-Salcedo, A., Kahn, B. H., Zelinka, M. D., . . . Wilkinson, J. (2019). Cloud feedbacks in extratropical cyclones: insight from long-term satellite data and high-resolution global simulations. *Atmos. Chem. Phys.*, 19(2), 1147–1172. doi: 10.5194/acp-19-1147-2019
- McCoy, D. T., Field, P. R., Schmidt, A., Grosvenor, D. P., Bender, F. A. M., Shipway, B. J., . . . Elsaesser, G. S. (2018). Aerosol midlatitude cyclone indirect effects in observations and high-resolution simulations. *Atmospheric Chemistry and Physics*, 18(8), 5821–5846. doi: 10.5194/acp-18-5821-2018
- McCoy, D. T., Hartmann, D. L., & Grosvenor, D. P. (2014, December). Observed Southern Ocean Cloud Properties and Shortwave Reflection. Part II: Phase Changes and Low Cloud Feedback*. *Journal of Climate*, 27(23), 8858–8868. doi: 10.1175/jcli-d-14-00288.1
- McCoy, D. T., Hartmann, D. L., Zelinka, M. D., Ceppi, P., & Grosvenor, D. P. (2015). Mixed-phase cloud physics and Southern Ocean cloud feedback in climate models. *Journal of Geophysical Research: Atmospheres*, 120(18), 9539–9554. doi: 10.1002/2015jd023603
- McCoy, D. T., Tan, I., Hartmann, D. L., Zelinka, M. D., & Storelvmo, T. (2016). On the relationships among cloud cover, mixed-phase partitioning, and planetary albedo in GCMs. *Journal of Advances in Modeling Earth Systems*, 8(2), 650–668. doi: 10.1002/2015ms000589
- Molod, A., Takacs, L., Suarez, M., & Bacmeister, J. (2015). Development of the GEOS-5 atmospheric general circulation model: evolution from MERRA to MERRA2. *Geoscientific Model Development*, 8(5), 1339–1356. doi: 10.5194/gmd-8-1339-2015
- Mulcahy, J. P., Jones, C., Sellar, A., Johnson, B., Boutle, I. A., Jones, A., . . . McCoy, D. T. (2018). Improved Aerosol Processes and Effective Radiative Forcing in HadGEM3 and UKESM1. *Journal of Advances in Modeling Earth Systems*, 0(0). doi: 10.1029/2018MS001464
- Myers, T. A., & Norris, J. R. (2016). Reducing the uncertainty in subtropical cloud feedback. *Geophysical Research Letters*, n/a–n/a. doi: 10.1002/2015GL067416
- Myers, T. A., Scott, R. C., Zelinka, M. D., Klein, S. A., Norris, J. R., & Caldwell, P. M. (2021, May). Observational constraints on low cloud feedback reduce uncertainty of climate sensitivity. *Nature Climate Change*. Retrieved from <https://doi.org/10.1038/s41558-021-01039-0> doi: 10.1038/s41558-021-01039-0
- Mülmenstädt, J., Salzmann, M., Kay, J. E., Zelinka, M. D., Ma, P.-L., Nam, C., . . . Quaas, J. (2021). An underestimated negative cloud feedback from cloud lifetime changes. *Nature Climate Change*, 11(6), 508–513. (Publisher: Nature Publishing Group)
- Qu, X., Hall, A., Klein, S. A., DeAngelis, & Anthony, M. (2015). Positive tropical marine low-cloud cover feedback inferred from cloud-controlling factors. *Geophysical Research Letters*, n/a–n/a. doi: 10.1002/2015GL065627
- Quaas, J. (2012). Evaluating the “critical relative humidity” as a measure of subgrid-scale variability of humidity in general circulation model cloud cover parameterizations using satellite data. *Journal of Geophysical Research: Atmospheres*, 117(D9), n/a–n/a. doi: 10.1029/2012JD017495
- Seager, R., & Henderson, N. (2013). Diagnostic Computation of Moisture Budgets in the ERA-Interim Reanalysis with Reference to Analysis of CMIP-Archived Atmospheric Model Data*. *Journal of Climate*, 26(20), 7876–7901. doi: 10.1175/JCLI-D-13-00018.1
- Senior, C. A., & Mitchell, J. F. B. (1993, March). Carbon-dioxide and Climate - The

- 562 Impact of Cloud Parameterization. *Journal of Climate*, 6(3), 393–418. doi: 10
563 .1175/1520-0442(1993)006(0393:cdacti)2.0.co;2
- 564 Sherwood, S. C., Webb, M. J., Annan, J. D., Armour, K. C., Forster, P. M., Har-
565 greaves, J. C., . . . Rohling, E. J. (2020). An assessment of Earth’s climate
566 sensitivity using multiple lines of evidence. *Reviews of Geophysics*, 58(4),
567 e2019RG000678.
- 568 Smith, R. N. B. (1990). A scheme for predicting layer clouds and their water con-
569 tent in a general circulation model. *Quarterly Journal of the Royal Meteorolog-
570 ical Society*, 116(492), 435–460. doi: 10.1002/qj.49711649210
- 571 Sousa, P. M., Blamey, R. C., Reason, C. J. C., Ramos, A. M., & Trigo, R. M. (2018,
572 December). The ‘Day Zero’ Cape Town drought and the poleward migration of
573 moisture corridors. *Environmental Research Letters*, 13(12), 124025. Retrieved
574 from <http://dx.doi.org/10.1088/1748-9326/aaebc7> (Publisher: IOP Pub-
575 lishing) doi: 10.1088/1748-9326/aaebc7
- 576 Stevens, B., & Brenguier, J. L. (2009). *Cloud controlling factors: Low clouds*. MIT
577 Press Cambridge, Mass.
- 578 Tan, I., & Storelvmo, T. (2019, March). Evidence of Strong Contributions
579 From Mixed-Phase Clouds to Arctic Climate Change. *Geophysical Re-
580 search Letters*, 46(5), 2894–2902. Retrieved 2021-03-06, from [https://
581 doi.org/10.1029/2018GL081871](https://doi.org/10.1029/2018GL081871) (Publisher: John Wiley & Sons, Ltd)
582 doi: 10.1029/2018GL081871
- 583 Terai, C. R., Klein, S. A., & Zelinka, M. D. (2016). Constraining the low-cloud
584 optical depth feedback at middle and high latitudes using satellite obser-
585 vations. *Journal of Geophysical Research: Atmospheres*, n/a–n/a. doi:
586 10.1002/2016JD025233
- 587 Terai, C. R., Zhang, Y., Klein, S. A., Zelinka, M. D., Chiu, J. C., & Min, Q. (2019).
588 Mechanisms Behind the Extratropical Stratiform Low-Cloud Optical Depth
589 Response to Temperature in ARM Site Observations. *Journal of Geophysical
590 Research: Atmospheres*, 124(4), 2127–2147. doi: 10.1029/2018jd029359
- 591 Tselioudis, G., Lipat, B. R., Konsta, D., Grise, K. M., & Polvani, L. M. (2016,
592 May). Midlatitude cloud shifts, their primary link to the Hadley cell, and their
593 diverse radiative effects. *Geophysical Research Letters*, 43(9), 4594–4601. doi:
594 <https://doi.org/10.1002/2016GL068242>
- 595 Tsushima, Y., Emori, S., Ogura, T., Kimoto, M., Webb, M. J., Williams, K. D., . . .
596 Andronova, N. (2006, August). Importance of the mixed-phase cloud distri-
597 bution in the control climate for assessing the response of clouds to carbon
598 dioxide increase: a multi-model study. *Climate Dynamics*, 27(2-3), 113–126.
599 doi: 10.1007/s00382-006-0127-7
- 600 Tukey, J. (1958). Bias and confidence in not quite large samples. *Ann. Math.
601 Statist.*, 29, 614.
- 602 Wentz, F. J., & Meissner, T. (2000). AMSR Ocean Algorithm, Version 2. *Remote
603 Sensing Systems, Santa Rosa, CA., report number 121599A-1*, 66 pp.
- 604 Wielicki, B. A., Barkstrom, B. R., Harrison, E. F., III, R. B. L., Smith, G. L.,
605 & Cooper, J. E. (1996). Clouds and the Earth’s Radiant Energy System
606 (CERES): An Earth Observing System Experiment. *Bulletin of the American
607 Meteorological Society*, 77(5), 853–868. doi: 10.1175/1520-0477(1996)077(0853:
608 catere)2.0.co;2
- 609 Wilson, D. R., Bushell, A., Kerr-Munslow, A. M., Price, J. D., Morcrette, C. J., &
610 Bodas-Salcedo, A. (2008). PC2: A prognostic cloud fraction and condensa-
611 tion scheme. II: Climate model simulations. *Quarterly Journal of the Royal
612 Meteorological Society*, 134(637), 2109–2125.
- 613 Yettella, V., & Kay, J. E. (2017). How will precipitation change in extratropical
614 cyclones as the planet warms? Insights from a large initial condition climate
615 model ensemble. *Climate Dynamics*, 49(5-6), 1765–1781.
- 616 Zelinka, M. D., Myers, T. A., McCoy, D. T., Po-Chedley, S., Caldwell, P. M.,

- 617 Ceppi, P., . . . Taylor, K. E. (2020, January). Causes of higher climate sen-
618 sitivity in CMIP6 models. *Geophysical Research Letters*, *n/a*(n/a). doi:
619 10.1029/2019GL085782
620 Zelinka, M. D., Zhou, C., & Klein, S. A. (2016). Insights from a refined decomposi-
621 tion of cloud feedbacks. *Geophysical Research Letters*, *43*(17), 9259–9269. doi:
622 10.1002/2016GL069917

623 **Figures**

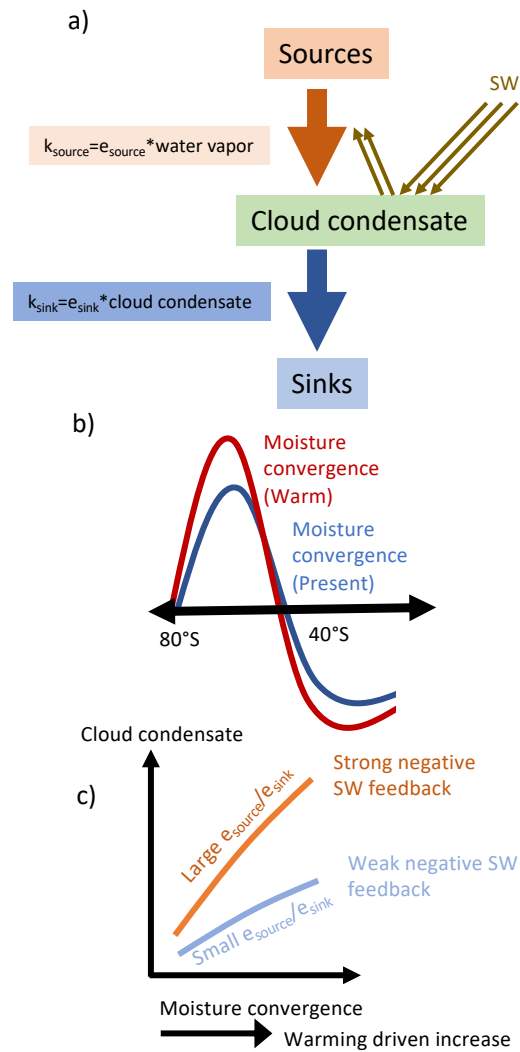


Figure 1. A schematic representation of the moisture convergence-cloud feedback mechanism examined in this study. (a) shows a hypothesized steady-state balance between sources and sinks of cloud. The rate of cloud creation is represented as k_{source} , which is conceptualized as an aggregate efficiency of cloud creation (e_{source}) multiplied by the reservoir of water vapor. The sink term k_{sink} is represented as a bulk sink efficiency (e_{sink}) multiplied by the reservoir of condensed water. (b) shows a cartoon of enhanced moisture convergence (approximated as $P - E$ in the text) in mean-state and warmed climate scenarios due to local and subtropical sources. Finally, (c) illustrates the resulting cloud condensate response to moisture convergence in the context of SW_{FB} . In GCMs where source efficiency is high relative to sinks the increase in LWP will be large resulting in a strongly negative SW_{FB} .

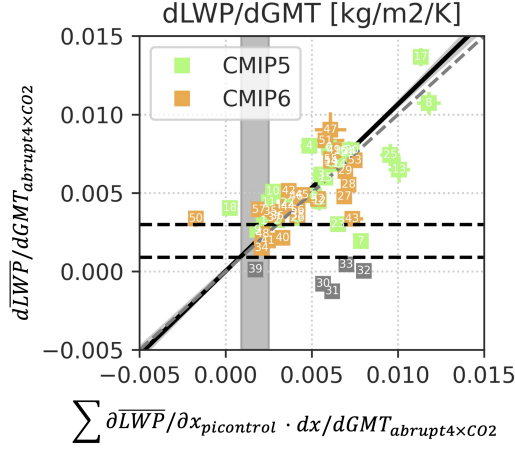


Figure 2. Prediction of the change in extratropical (40-85°S) \overline{LWP} during CO_2 quadrupling from Eq. 2. LWP response is normalized by GMT. The best fit line is shown in black with uncertainty in the best fit in grey shading. The 1-1 line is shown in dashes. Grey markers are not used in the fit (see text for details). The observational constraint is shown as a grey box on the x-axis and the intersection with the fit line is shown using horizontal dashed lines.

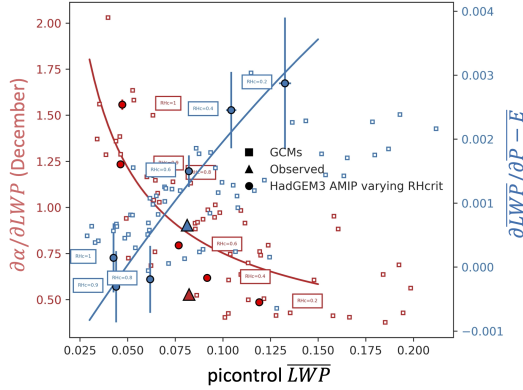


Figure 3. Radiative efficiency ($\partial\alpha/\partial LWP$) and moisture sensitivity ($\partial\overline{LWP}/\partial P - E$) anti-correlate across GCMs as a function of mean state extratropical \overline{LWP} . Observations from CERES, MERRA-2, and MAC-LWP are shown using triangles. Simulations in HadGEM3 perturbing source strength (RH_{crit} is noted in boxes) are shown as circles. A powerlaw is used to fit $\partial\alpha/\partial LWP$ and a second order polynomial is used to fit $\partial\overline{LWP}/\partial P - E$.

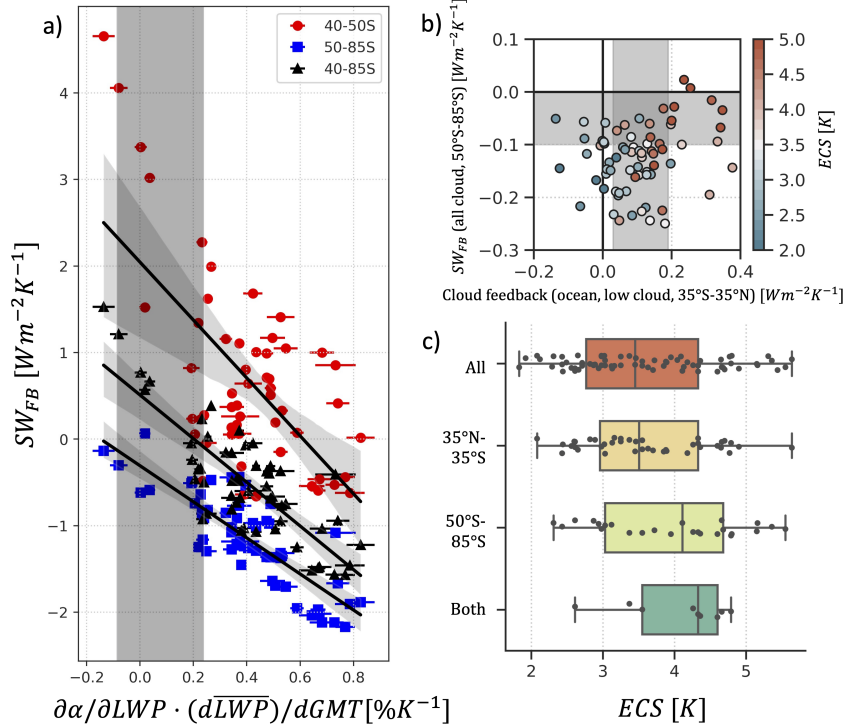


Figure 4. (a) SW cloud feedback (SW_{FB}) as a function of the predicted response of 40-85°S \overline{LWP} to GMT ($d\overline{LWP}/dGMT$, Fig. 2) scaled by the sensitivity of α to LWP ($\partial\alpha/\partial LWP$, Fig. 3). SW_{FB} is weighted by global surface area. The range consistent with observations is shown as a shaded grey box and the best fit regression and 95% confidence on the fit are shown using a black line and grey shading. SW_{FB} is shown averaged over three regions: 40-50°S (drying driven by Hadley cell expansion), 50-85°S (the region of consistent moistening), and 40-85°S. (b) the distribution of 50-85°S SW_{FB} and 35°S-35°N total marine low cloud feedback in CMIP5 and CMIP6 GCMs colored by ECS. Observational constraints from this study (y-axis, panel (a)) and consistent with Myers et al. (2021) (x-axis) are shown as grey shading. (c) the effects on the distribution of ECS in CMIP5 and CMIP6 of removing GCMs not consistent with the constraints shown in (b). The effect of constraining the prior distribution of models by subtropical and extratropical constraints from (b) are shown along with the result of applying both constraints at once.